Comparative study of multiaxial fatigue methods applied to welded joints in marine structures

P.S. van Lieshout, J.H. den Besten, M.L. Kaminski
Delft University of Technology, Netherlands
P.S.vanLieshout@tudelft.nl, Henk.denBesten@tudelft.nl, M.L.Kaminski@tudelft.nl

ABSTRACT. Marine structures are particularly prone to action of waves, winds and currents with stochastically varying composition, intensities and directions. Therefore, resultant stresses may cause multiaxial fatigue in specific welded structural details. For the assessment of multiaxial fatigue in welded joints, a wide variety of methods have been suggested. However, there is still no consensus on a method which can correctly account for non-proportional and variable amplitude loading. This paper beholds a comparative study of multiaxial fatigue methods applicable for design of marine structures. For the purpose of comparison several load cases were defined including non-proportional and variable amplitude loadings with different normal and shear stress amplitude ratios. Three types of methods are compared: those described by three different codes (i.e. Eurocode 3, IIW and DNV-GL), those described by three different multiaxial fatigue approaches from literature (i.e. Modified Carpinteri-Spagnoli Criterion, Modified Wohler Curve Method and Effective Equivalent Stress Hypothesis) and an approach based on Path-Dependent-Maximum-Range multiaxial cycle counting. From this study it has been concluded that non-proportional variable amplitude loading has a significant negative impact on the fatigue lifetime estimates, and that further research and experimental testing are essential to come to a consensus.

KEYWORDS. Multiaxial fatigue; Welded joints; Marine structures; Non-proportional; Variable amplitude loading; Constant amplitude loading.

INTRODUCTION

Most welds in structural details of marine structures are predominantly subjected to uniaxial stresses due to the stiffness distributions in typical structural member assemblies like stiffened panels, frames and trusses. However, there are also welds which could be subjected to multiaxial stresses induced either by geometry [1, 2] or loading. Such stresses may lead to a significant reduction of the fatigue resistance of welded steel [3]. Considering that the majority of marine structures are (relatively thick) plated structures, such fatigue lifetime reductions are generally caused by the combined effect of a dominant normal and shear stress (mixed Mode-I and Mode-III).

Currently, fatigue design of marine structures is predominantly based on uniaxial fatigue criteria assuming a governing Mode-I. These criteria are then used in combination with a damage accumulation hypothesis (e.g. Miner's rule) and cycle counting method (e.g. rainflow counting) to determine the fatigue lifetime. However, such an approach can be non-conservative for structural details where the welds are subjected to multiaxial stresses, especially when these are non-proportional, i.e. out-of-phase (OP).

Over the last few decades intensive efforts have been made to develop multiaxial fatigue approaches which are able to deal with difficulties such as (random) variable amplitude (VA) loading and non-proportionality. This has resulted,

amongst others, in multiaxial cycle counting methods [4-6], critical plane based criteria [3, 7- 9] , invariant based criteria [10] and energy based criteria [11]. Furthermore, spectral methods have been developed to assess multiaxial fatigue in the frequency domain, instead of the time domain [12]. However, still no consensus has been reached on an approach for the assessment of multiaxial fatigue in welded joints, whereby non-proportionality and variable amplitude loading can be accounted for correctly [13].

This study aims to identify the discrepancies resulting from the use of different multiaxial fatigue approaches for the fatigue analysis of welded joints in marine structures, considering proportionality and stress amplitude (ratio). The comparative study has been carried out using several conceptual constant (CA) and variable amplitude load cases. Each CA case has been analysed using three different codes and three multiaxial fatigue methods from literature. The VA cases have been analysed with an approach based on PDMR multiaxial cycle counting.

THEORETICAL BACKGROUND

When analysing the fatigue performance of a marine structure (i.e. ship or offshore structure) there are three preliminary steps which can be distinguished:

1. Hydrodynamic analysis;
   The structural response is induced by exposure to (multiaxial) environmental loads (e.g. wind, current and waves) and operational loads. Confused sea states and/or joint geometry can hereby lead to multiaxial stress states. With a hydrodynamic analysis the loads can be converted into time series or response transfer functions, consisting of RAOs (Response Amplitude Operators) and phase angles, which describe the structural behaviour in all six degrees of freedom.
2. Structural analysis;
   Multiaxial stress states can be induced depending on the (combination of) loading and structural geometry at global and local level. In order to identify the locations where such multiaxial stresses occur, it is often required to execute a global and local structural analysis.
3. Fatigue analysis;
   Stress or strain time trace histories can be extracted (in a time domain analysis) or generated (in a frequency domain analysis) with the structural analysis and subsequently be used to estimate the fatigue performance of the structure.

A multiaxial fatigue analysis is not a procedure with a univocal set of instructions. In fact, different decisions can be made at four elementary levels. In the first place it is of importance to narrow down the possibilities by defining the domain (time or frequency), joint type (welded or non-welded), material characteristics (ductile, semi-ductile or brittle) and scale (macro, meso or micro). This leads to the second level where it has to be decided whether an intact geometry parameter will be chosen, wherefore SN-curves will be used, or a crack damaged parameter, whereby fracture mechanics will be used [14].

Marine structures typically deal with high cycle fatigue whereby fatigue crack initiation dominates the total fatigue life. This fatigue regime is generally described by stress ranges due to the fact that low stress amplitudes are encountered which cause elastic deformation of the material [15]. On the other hand, elastic-plastic deformations induce low cycle fatigue and is therefore generally described by strain ranges. An intact geometry parameter is most commonly applied for the fatigue design of welded joints in marine structures. Generally, a fail-safe design approach is followed, meaning that the structural integrity can cope with the failure of an individual member [14, 15]. Such a design approach is chosen because it is anticipated that imperfections are present in the material, induced by production and/or welding.

Using an intact geometry parameter, a distinction can be made between those who lead to a fatigue lifetime estimate (i.e. finite lifetime) and those who identify a 'safe region' without fatigue crack initiation (i.e. an infinite lifetime). This 'safe region' is then identified by a fatigue boundary definition. An example of such a definition is the Dang Van criterion [16-19]. However, to obtain a fatigue lifetime estimate four steps have to be undertaken. In this fourth elementary level the fatigue damage parameter(s) should be identified (i.e. stress, strain or energy-a product of stress and strain) including the basis on which these parameters are being considered (i.e. a critical plane, an invariant, an integral). Then, the cycle counting procedure (uniaxial or multiaxial), damage rule (linear of non-linear) and the reference SN-curve (considering separate modes or mixed modes) have to be chosen. In Fig. 1 a schematic overview is given of the four elementary levels of decision making indicating the different options.

One of the difficulties with multiaxial fatigue in welded marine structures is that the phenomenon of fatigue in welded joints cannot be scaled. Plenty of research on multiaxial fatigue has been executed for the automotive and aerospace

industry but this knowledge, concerning thin plated structures, cannot be directly transferred to relatively thick plated marine structures. As elaborated in [15], fatigue resistance decreases with increasing plate thickness due to an increase in welded material volume, residual stress effects, surface quality and a larger stressed material volume. A total stress concept was developed to incorporate these effects. However, this concept was developed for welded Aluminium joints subjected to uniaxial fatigue and has not yet been extended to steel joints facing multiaxial fatigue.

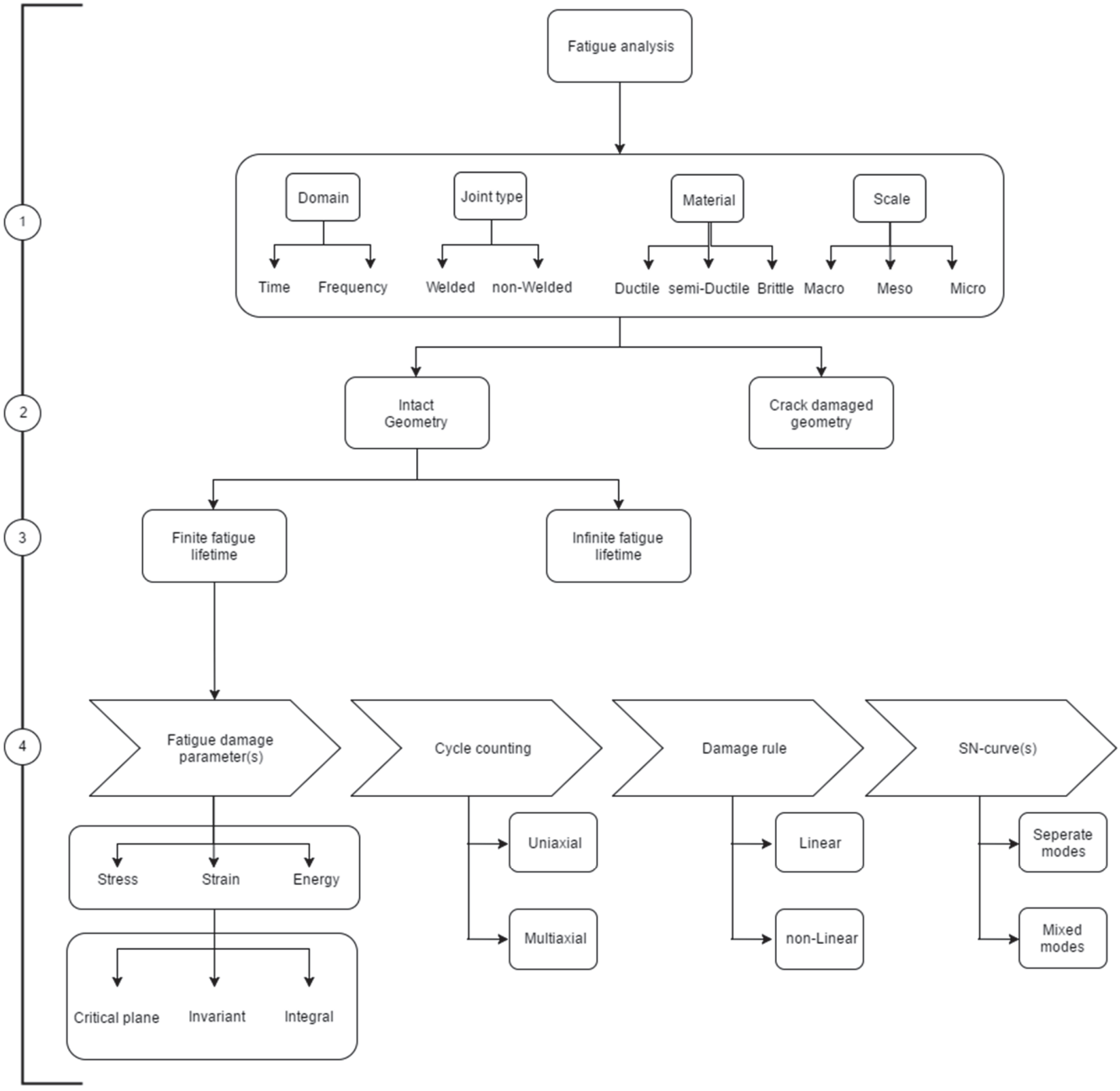

Figure 1: Overview of the four elementary levels in a multiaxial fatigue analysis.

In literature different fatigue damage models can be found which describe fatigue crack evolution as a combination of shear stress dominated crack initiation and normal stress dominated crack growth e.g. Miller's 2-Stage concept and Socie's damage model [20]. This is based on the physical phenomenon whereby Persistent Slip Bands (PSB's) form when a crystal is subjected to microscopic cyclic stresses. PSB's are parallel to the easy glide material plane which has, for example for Mode I loading, typically a 45 degrees inclination with the normal. PSB's facilitate laminar flow under shear loading which

causes the initiation of a fatigue crack: they follow the path of the least resistance. Once a micro-crack has been formed the microscopic stress concentration moves with the crack tip until the crack reaches its next slip band. This also explains the +/- 45 degrees zig-zag crack profile that is often observed at micro- or meso-scale. Therefore, fatigue crack initiation is shear stress governed and fatigue crack growth normal stress governed. At macro-scale the average profile is 0 degrees meaning perpendicular to the principal stress (and equal to the normal stress for a mode-I loading). Therefore, fatigue crack initiation (at micro and meso scale) is shear stress governed and fatigue crack growth at macro-scale normal stress governed. Moreover, this holds for different cracking modes. This is the underlying theory for including a normal and shear stress component in multiaxial fatigue models which aim to determine fatigue lifetime (i.e. fatigue crack initiation and growth).

MULTIAXIAL FATIGUE METHODS IMPLEMENTED IN CODES

Amongst the codes which have been developed for the fatigue design of marine structures e.g. Eurocode 3, IIW, DNV-GL-0005, two types of approaches can be distinguished. They use either standardized interaction equations or the maximum principal stress (together with its relative direction with respect to the weld toe) [21-23]. The SN-curves that are used in combination with these recommended approaches are obtained from experimental tests and are presented independent of a mean stress [24]. This is based on the presumption of high tensile residual stresses in the weld [19].

Interaction equations originate from the empirical finding that under combined bending and torsional loading ductile materials (e.g. steel) show an ellipse shape of the fatigue limits in the normal/shear stress diagram [25-26]. This eventually resulted in the well-known empirical Gough-Pollard equation (i.e. Gough ellipse), see Eq. 1. For brittle materials this was not an ellipse shape but a parabola. Therefore, the exponent of the normal stress term in the Gough-Pollard equation could be considered as a function of (the ratio of) the fatigue limits. This leads into the generic ellipse arc formulation provided in Eq. 2 [27].

$$\left(\frac{\sigma}{\sigma_{A,-1}}\right)^2+\left(\frac{\tau}{\tau_{A,-1}}\right)^2=1 \tag{1}$$

$$\left(\frac{\sigma}{\sigma_{A,-1}}\right)^k+\left(\frac{\tau}{\tau_{A,-1}}\right)^2=1 \tag{2}$$

$$k=f\left(\frac{\sigma_{A,-1}}{\tau_{A,-1}}\right)$$

Principal stress based approaches were developed from the experimental observation that fatigue cracks grow normal to the principal stress direction when it has a constant directionality [21]. This observation was then also used as a basis for the assessment of multiaxial fatigue with changing principal stress direction (e.g. non-proportionality). The size and orientation of the principal stress direction are then taken into account.

Eurocode 3

For the fatigue design of steel structures, The European Union has established Eurocode-3. This code advises to account for the combined effect of the normal and shear stress components, acting respectively perpendicular and parallel to the weld toe, through an interaction equation (Eq. 3). In order to establish this relationship fatigue tests from large scale specimens were used, including geometrical and structural imperfections from material production. The constant amplitude equivalent normal stress range $\Delta\sigma_{eq}$ and shear stress range $\Delta\tau_{eq}$ are related to the design resistances $\Delta\sigma_R$ and $\Delta\tau_R$ defined at a certain number of stress cycles for a particular detail category. It can be seen from Eq. 3, that two individual damage mechanisms are incorporated: two different exponents are used for respectively the normal stress term and the shear stress term. The selected values for the exponents originate from the fatigue resistance to shear stress which typically shows a slope of 5 and for normal stress a slope of 3. This diverges from the exponents suggested in the Gough-

Pollard equation (Eq. 1). However, it was concluded in a comparative study executed by [25] that Eurocode 3 provides consistently less accurate results in comparison to two other interaction equations which use the exponents as suggested in the Gough-Pollard equation (i.e. IIW and SFS 2378). Particularly for non-proportional combined loading, differences are observed when compared to experimental data from welded joints. It is therefore questionable whether the individual damage mechanisms remain unaffected by combined load cases.

$$\left(\frac{\Delta\sigma_{eq}}{\Delta\sigma_R}\right)^3+\left(\frac{\Delta\tau_{eq}}{\Delta\tau_R}\right)^5\le 1 \tag{3}$$

IIW

Based on experimental investigations and recommendations from contributing researchers the International Institute of Welding (IIW) developed a similar relationship between the normal and shear stress component as Eurocode 3. However, in comparison to Eurocode 3, the interaction equation as defined by the IIW seems more advanced: Eq. 4. The code allows for different material ductility (steel or aluminium), load characteristics (CA and VA loading, both in combination with either in-phase (IP) or OP loading), and a correction for fluctuating mean stress. For each particular case a critical Miner's damage sum (equating to $0.2;0.5\,\text{or}\,1$) and comparison value $CV\left(0.5\,\text{or}\,1\right)$ is advised. The design resistance of particular detail category is expressed by FAT class. Similar to the Gough-Pollard equation (Eq. 1) there is no difference observed between the two damage mechanisms (i.e. shear and normal stress induced): both terms in the equation are raised to power of two. However, the interaction effect can be (partially) covered by the CV value and maximum damage sum that are used in the fatigue analysis.

$$\left(\frac{\Delta\sigma_{eq}}{\Delta\sigma_R}\right)^2+\left(\frac{\Delta\tau_{eq}}{\Delta\tau_R}\right)^2\le CV \tag{4}$$

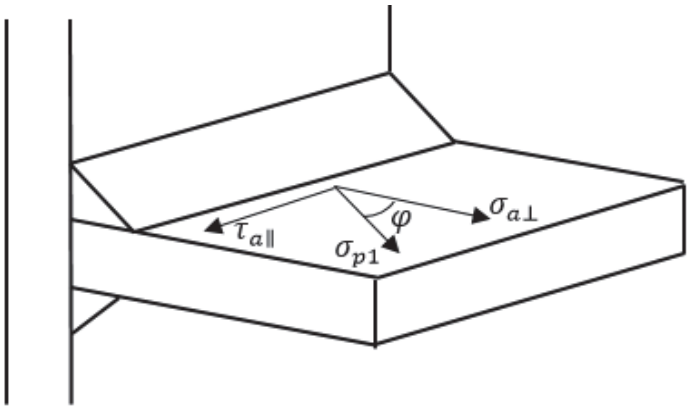

Figure 2: Illustration clarifying how angle φ is used to determine the maximum principal stress direction σ_{p1} with respect to the weld toe; Reproduced from [21].

DNV-GL-RP-0005

DNV-GL has established a recommended practice for fatigue design of offshore steel structures based on the maximum principal stress and its direction. The use of principal stresses in the DNV recommended practice for marine structures originates from 1984 and originates from experimental observations that fatigue cracks grow perpendicular to the principal stress direction for uniaxial and proportional multiaxial load cases (i.e. the load cases where the direction of the principal stress doesn't change (during one load cycle)). Therefore, the direction of the principal stress range is taken into account by an angle φ between the maximum principal stress σ_{p1} and the normal to the weld toe $\sigma_{a\perp}$ (see Fig. 2). Once this angle exceeds a critical value, the notch at the weld toe may no longer be the critical location for fatigue. A higher reference SN-curve is then recommended depending on the detail category [21]. It should be noted that the same approach is considered applicable to non-proportional load cases whereby the principal stress changes direction in one load cycle. Important to note is the fact that the fatigue assessment following this recommended practice is Mode I based

i.e. the angle relative to the normal of the weld seam is being considered. The interaction effect between Mode I and Mode III is not taken into account.

MULTIAXIAL FATIGUE METHODS FROM LITERATURE

Multiaxial fatigue methods are often categorized on the basis of their fatigue damage parameter(s) and their approach, cf. Section 2. Critical plane based methods are considered promising for the analysis of multiaxial fatigue problems because they show good correlation with experimental observations [28]. Moreover, they can incorporate non-proportionality and distinguish between phase shift induced non-proportionality and frequency induced non-proportionality. They originate from experimental observations where fatigue crack initiation (i.e. nucleation and early growth) appeared to occur on preferred material planes [29]. However, these observations were made in non-welded smooth specimens. Many critical plane based methods were therefore originally developed for smooth and notched specimens. However, in welded joints the crack initiation and early crack growth phase are affected by the welding process. Nowadays, several critical plane based methods have been explicitly developed or extended for welded joints. However, it is often not clear in literature in how far these approaches can be applied to multiaxial fatigue problems in welded joints.
Instead of identifying a particular critical plane it is suggested by some approaches to consider the interaction between the different material planes through integration. On these grounds, three methods have been selected for further investigation.

Modified Carpinteri-Spagnoli Criterion

The Modified Carpinteri-Spagnoli Criterion was originally found suitable for smooth and blunt notched specimens [30] and later extended for welded joints facing multiaxial fatigue [7]. The basis of the original criterion are experimental observations which demonstrated a correlation between the fatigue crack plane and the direction of the maximum principal stresses/strains and maximum shear stress/strain [30]. Two stages were distinguished: shear stress driven crack initiation and fatigue crack growth in the plane normal to the direction of the maximum principal stress. Interestingly, this criterion combines the different approaches that are suggested in the design codes (cf. Section 3) by suggesting an interaction equation which considers the stress components acting on a critical plane which is directly related to the averaged principal stress direction.
The Modified Carpinteri-Spagnoli Criterion (MCSC) is formulated as a quadratic combination of the maximum normal stress amplitude and shear stress amplitude acting on the critical plane [31]:

$$\left(\frac{\sigma_{max}}{\sigma_{A,-1}}\right)^2+\left(\frac{\tau_A}{\tau_{A,-1}}\right)^2\le 1 \tag{5}$$

$\sigma_{A,-1}=$ *fully reversed normal stress fatigue limit for bending* $(\mathrm{R}=-1)$
$\tau_{A,-1}=$ *fully reversed shear stress fatigue limit for torsion* $(\mathrm{R}=-1)$

In order to define the directions of the averaged principal stresses it was initially suggested to apply an averaging procedure using weight functions which would result in three Euler angles (θ,ψ,ϕ) determining the orientation of each averaged principal stress. However, from a parametric study it was found that the averaged principal stress direction almost coincides with the moment where the principal stress reaches its maximum value in a load cycle. This simplified the original calculation procedure [7]. In Fig. 3a it can be seen how the directions of the averaged principal stresses (whereby $Z'=\hat{1},\ X'=\hat{2},Y'=\hat{3}$) are defined using the three Euler angles ϕ,θ and ψ which correspond to counter clockwise rotations about respectively the Z-axis, the so called line of nodes N and the Z'-axis (i.e. rotated Z-axis) [32].
Based on experimental observations an empirical expression was formulated for the off angle δ (resulting from a clockwise rotation around the $\hat{2}$ axis) between the normal to the critical plane w and the averaged direction of the maximum principal stress $\hat{1}$. The empirical expression for δ is given in Eq. 6. Furthermore, an additional counter clockwise angle about w is formulated. This angle γ. enables to described the local coordinate system by the axes uvw as illustrated in Fig. 3b.

Different methods have been developed to determine the shear stress amplitude acting on a critical plane. In this comparative study the Minimum Circumscribed Circle method was used. This method has been described in [7, 31, 33].

$$\delta = 45\frac{3}{2}\left[1-\left(\frac{\tau_{af,-1}}{\sigma_{af,-1}}\right)^2\right] \tag{6}$$

$$whereby \frac{1}{\sqrt{3}} < \frac{\tau_{af,-1}}{\sigma_{af,-1}} < 1$$

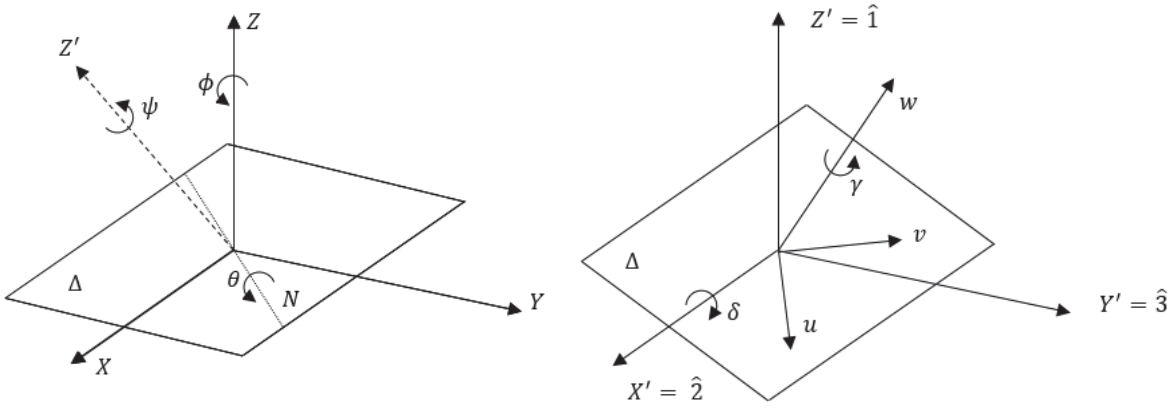

Figure 3: Representation of the counter clockwise rotations about the Z,N and Z'axis, defined through three Euler angles θ,ψ,ϕ (a) Relationship between the two spherical angles δ and γ with respect to the local coordinate system with axes uvw (b); Reproduced from [32].

Modified Wohler Curve Method

The MWCM considers the normal and shear stress components acting on a particular critical plane whereby the orientation of the critical plane is determined by a Maximum Variance Method (MVM). This MVM is based on the experimental observation that fatigue damage shows proportionality with the variance of a random uniaxial load signal, both for Gaussian and non-Gaussian loadings [34]. Therefore, the critical plane corresponds to the material plane which coincides with the direction along which the variance of the resolved shear stress is maximum. The complexity of the stress state is then expressed by the stress amplitude ratio $\rho = \Delta\sigma_n / \Delta\tau$ which indicates the degree of non-proportionality. Hereby, σ_n is the normal stress acting perpendicular to the critical plane and τ is the resolved shear stress acting on the critical plane.

The MWCM presumes that fatigue damage is independent of the (nominal) load path as long as the stress ratio and shear stress range relative to the critical plane are the same. Therefore, a linear relationship is suggested for the construction of a modified load specific SN-curve [34]. Fig. 4 illustrates how this load specific SN-curve is constructed based on the tension and torsional fatigue curves. The equations that represent this linear relationship are given in Eq. 7 and 8.

$$\left(\frac{\Delta\sigma_A}{2}-\Delta\tau_A\right)\cdot\rho + \Delta\tau_A = \Delta\tau_{A,ref}(\rho) \tag{7}$$

$$\left(k-k_0\right)\cdot\rho + k_0 = k_\tau(\rho) \tag{8}$$

The MVM describes the orientation of the critical plane using two polar angles φ and θ with respect to the local *nab* coordinate system of the critical plane. The angle θ represents the angle between the normal to the critical plane and the Z-axis of the global reference coordinate system, while angle φ represents the angle between the projection of the normal

n to the critical plane on the XY-plane in the global reference coordinate system. In addition, angle α is used to determine the orientation of the shear stress vector in the critical plane which corresponds with the maximum resolved shear stress along unit vector q. Fig. 5a and 5b elucidates how the three angles φ,θ and α are related to the critical plane and its local coordinate system.

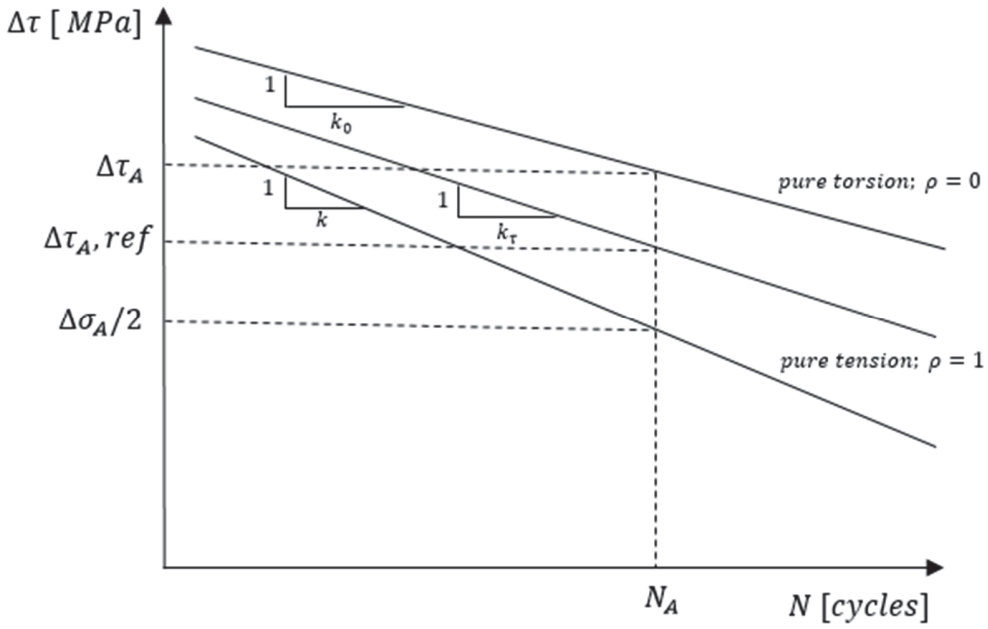

Figure 4: Constructing a load specific SN-curve using the curves for pure uniaxial and torsional loading following the Modified Wohler Curve Method; Reproduced from [9].

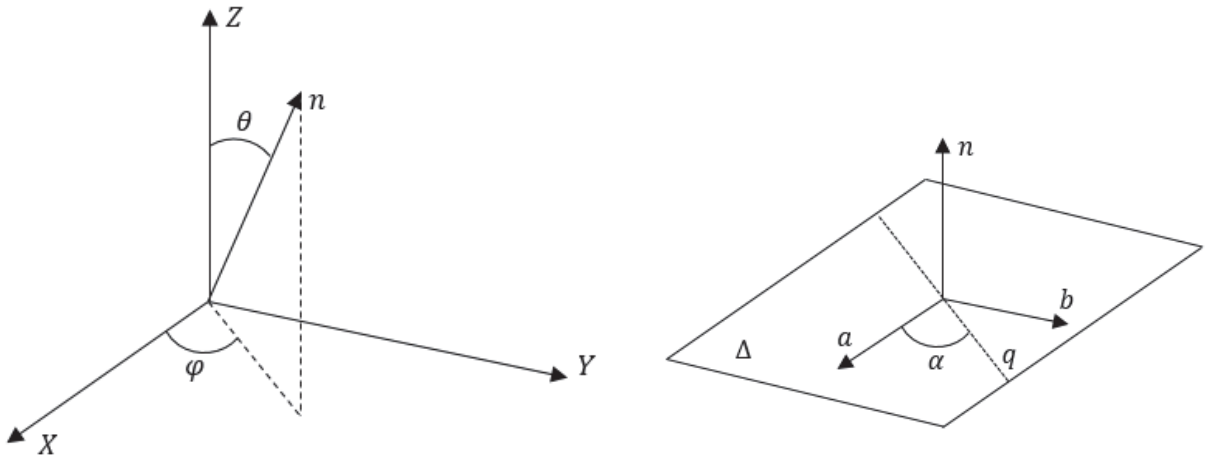

Figure 5: Determination of the orientation of the normal to the critical plane using the angles φ and θ (a) Determination of the orientation of the local coordinate system of the critical plane abn using angle α; (b) Reproduced from [35].

Effective Equivalent Stress Hypothesis

From previous research it was concluded that the Von Mises equivalent stress encounters difficulties with non-proportional multiaxial loadings [3, 36]. The EESH was developed with the aim to improve the Von Mises equivalent stress formulation for cases of non-proportional multiaxial fatigue. The hypothesis tries to incorporate the detrimental effect of non-proportional loading on fatigue lifetime by considering the interaction of shear stress in different material planes. This is based on the consideration that for ductile materials shear stress initiates multiaxial fatigue failure . The maximum local stress in the weld toe is hereby presumed governing for fatigue life. Therefore, the approach uses local stresses.

Originally, [3] included a square root term in the hypothesis to try to account for the influence of the maximum stressed material volume on the local stress. However, this term was found to be unsuccessful and got removed from the equation [37]. The EESH defines a local equivalent stress σ_{EESH}, based on the Von Mises stress equivalent which is determined as a function of the phase angle δ (see Eqs. 9-10).
The interaction of the shear stresses acting at different material planes is incorporated by an effective shear stress term F which is also a function of the phase angle δ. The effective shear stress is an integral of all shear stress components (i.e. τ_n) acting on the material planes (in two dimensional space) defined by their angle of rotation φ. Due to this integration procedure frequency induced non-proportionality is also covered in this hypothesis. However, as can be seen from Eq. 11, the calculations become significantly more complex once variable amplitude loading is encountered.
Henceforth, damage calculation requires a local SN curve. Such a local SN-curve was constructed with experimental data from a welded flange-tube specimen in Sonsino & Kueppers (2001).

$$\sigma_{EESH}(\delta)=\sigma_{EESH}(\delta=0)\cdot\frac{F(\delta)}{F(\delta=0)} \tag{9}$$

$$\sigma_{EESH}(\delta=0)=\sqrt{{\sigma_x}^2+{\sigma_y}^2-\sigma_x\cdot\sigma_y+3{\tau_{xy}}^2} \tag{10}$$

$$F(\delta)=\frac{1}{\pi}\int_0^{\pi} f_p(\varphi)\,d\varphi \tag{11}$$

$$f_p(\varphi)=\begin{cases}\text{for constant amplitude loading}:\tau_n(\varphi)\\ \text{for variable amplitude loading}:\dfrac{1}{L_s}\displaystyle\sum_{i=1}^{L_s}\tau_{n,i}(\varphi)\end{cases}$$

whereby L_s = *sequence length of the load spectrum*

COMPARATIVE STUDY

The stress state at a location of interest can be analyzed at different levels. In the current literature different methods have been developed based on nominal stress [38, 9], hot spot stress [38-41] or structural stress [42-44] and notch stress [19, 45-47]. They differentiate amongst one another in the amount of local stress information. The nominal stress approach only considers the membrane component of stress induced by the macro-geometry of the joint, excluding stress concentrations [23]. The hot spot or structural stress approach considers an equilibrium-equivalent structural stress part as a composition of a membrane and bending stress component. It uses linear extrapolation towards the weld toe in order to account for the membrane and bending component of stress (or through-thickness linearization), excluding the effect of the notch at the weld-toe transition. This means that only those stress concentrations are being considered which are caused by the structural detail of the joint [40]. The effective notch stress approach accounts for the additional stress peak induced by the notch at the weld-toe transition (i.e. self-equilibrating notch stress part). Typically, the more local information is added the more accurate the fatigue lifetime estimates should become. However, at a certain point it is no longer worthwhile to add more local information because it cannot overcome statistical scatter in experiments [14].
This comparative study is based on nominal stresses. The reasoning behind this is that more local stress information (e.g hot spot/structural stress, notch stress) would require a specified joint geometry. The objective is to execute a comparative study which is independent of joint dimensions. Moreover, the results can be considered conservative because more local stress information would improve the accuracy.

Constant amplitude loading

Five different conceptual CA load cases have been established presuming harmonic sinusoidal loading, see Tab. 1. The stress amplitude ratio was set to $\sigma_A/\tau_A=1/\sqrt{3}$ (with a normal stress amplitude of $\sigma_A=100\,MPa$) and a frequency ratio of $f_\sigma/f_\tau=1$. Load case 5 is an exception whereby the frequency ratio is set to 2.

Reference SN-curves had to be selected for each code separately. For this purpose a non-load carrying fillet welded joint was presumed leading to CAT 80, FAT 80 and E Category for Eurocode 3, IIW and DNV-GL respectively. The reference SN curves were used to find the number of cycles N_f which meet the established criterion and were then transposed to fatigue damage using Miner's rule [48]. For LC 5 two different strategies have been applied. The first one is a conservative interpretation (referred to as LC 5.1), whereby the frequency of the normal stress component is presumed similar to the shear stress component (i.e. twice as high as actually is the case). The second strategy (referred to as LC 5.2) accounts the actual number of cycles of the shear stress component when finding agreement with the fatigue criterion. All damage sums have been normalized with the pure Mode-I load case (i.e. LC 1), for each code separately, and are listed in Tab. 2a.

Load case 1 (LC 1) *- Pure tension -*	Load case 2 (LC 2) *- Pure torsion -*	Load case 3 (LC 3) *- Tension & Torsion - In-phase*	Load case 4 (LC 4) *- Tension & Torsion - Out-of-phase*	Load case 5 (LC 5) *- Tension & Torsion - Out-of-phase*
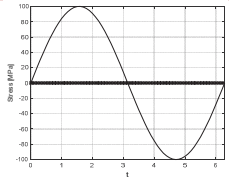	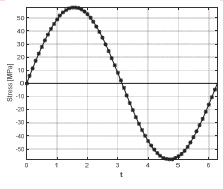	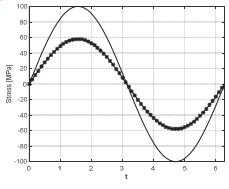	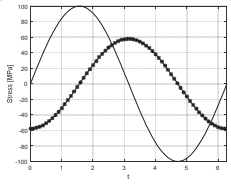	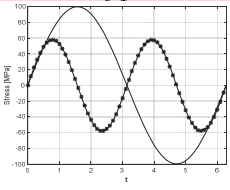

Table 1: Definition of CA load cases

Code	LC 1	LC 2	LC 3	LC 4	LC 5	
					LC 5.1	LC 5.2
Eurocode 3	1.0	0.41	1.4	1.4	2.8	1.8
IIW	1.0	0.41	2.6	9.8	20	3.5
DNV-GL-RP-0005[1]	1.0	0.14	1.1	1.0	1.0	

Table 2a: Normalized effect of stress multiaxiallity on fatigue damage predicted using selected codes – Comparison between the different load cases.

For the three selected multiaxial fatigue methods, particular reference SN-curves had to be used. For this purpose experimental data collected by [3] was used. Run-outs were excluded. The use of this data set is favourable as the stress concentration factors for bending and torsion of this test specimen are known.
This enables to determine the local stresses at the weld which are needed for application of the EESH. To determine fatigue damage a reference SN-curve based on the local equivalent stress amplitude could now be used. This SN-curve was defined earlier by [3]. For the MCSC and MWCM the pure Mode-I and pure Mode III curve were used [34]. All normalized damage sums are listed in Tab. 2b. It should be emphasized that the results listed in Tabs. 2a and 2b show the relative differences between the different load cases.

Critical plane method	LC 1	LC 2	LC 3	LC 4	LC 5
MCSC	1.0	0.15	2.7	2.3	2.7
MWCM	1.0	0.15	1.2	1.3	1.3
EESH	1.0	0.02	1.7	2.5	4.4

Table 2b: Normalized effect of stress multiaxiallity on fatigue damage predicted using selected multiaxial fatigue methods

In addition, the codes and methods have been compared amongst each other for each individual load case. In Tab. 3a the results from the selected codes are listed after normalization with the lowest fatigue damage. From the three selected

[1] Considering an in air environment

multiaxial fatigue methods only the results from MCSC and MWCM were considered because they use the same reference SN-curve. Including the results obtained with the EESH would not be just because this method is based on a local approach. The results were normalized with the lowest fatigue damage and are listed in Tab. 3b.

Variable amplitude loading – Case study

In various previous studies on the applicability and validity of multiaxial fatigue methods conceptual load histories have been used [49-51]**.** However, difficulties start to arise when it is intended to execute a multiaxial fatigue analysis on a structure under OP VA loading, which is representative for the actual day-to-day loading on marine structures. For this purpose a case study was developed by the authors and was then used to investigate the effect of stress amplitude ratio on fatigue damage using PDMR based multiaxial cycle counting [52].

Code	LC 1	LC 2	LC 3	LC 4	LC 5	
					LC 5.1	LC 5.2
Eurocode 3	1.0	3.0	1.3	1.4	2.7	1.7
IIW	1.0	3.0	2.4	9.8	19	3.3
DNV-GL-RP-0005[2]	1.0	1.0	1.0	1.0	1.0	

Table 3a: Normalized effect of stress multiaxiallity on fatigue damage predicted using selected codes – Comparison between the different codes.

Critical plane method	LC 1	LC 2	LC 3	LC 4	LC 5
MCSC	1.0	1.0	2.3	1.7	2.0
MWCM	1.0	1.0	1.0	1.0	1.0

Table 3b: Normalized effect of stress multiaxiallity on fatigue damage predicted using selected multiaxial fatigue methods – Comparison between the different methods.

Marine structures are in reality subjected to a combination of stationary sea states whereby each sea state consists of one, two or several wave systems [53]. Each wave system is then defined by a spectral density function. Simultaneous wind seas and swells generally dominate the wave spectrum of floating marine structures.

However, as a simplified approach, Zou & Kaminski (2016) suggest to use one expression to represent all swells by a particular spectrum with a mean wave direction. This suggestion is based on wave energy conservation The same assumption can be made for wind seas. In this case study this simplified approach has been followed. Wind driven seas were described by the mean JONSWAP spectrum as advised by the 17th ITTC in 1984 [54] and swell sea by a Gaussian swell spectrum (see Eqs. 8 and 9).

$$S_{JONSWAP}(\omega) = \frac{320 H_{s,wind}^{2}}{T_{p,wind}^{4}} \cdot \omega^{-5} \cdot exp\left\{-\frac{1950}{T_{p,wind}^{4}} \cdot \omega^{-4}\right\} \cdot \gamma^{A} \tag{8}$$

$$whereby\ A = exp\left\{-\left(\frac{\frac{\omega}{\omega_{p,wind}} - 1}{\sigma\sqrt{2}}\right)^{2}\right\}; \omega_{p,wind} = \frac{2\pi}{T_{p},wind}; \sigma = \begin{cases} 0.07\ if\ \omega < \omega_{p} \\ 0.09\ if\ \omega > \omega_{p} \end{cases}$$

$$S_{Gaussian}(\omega) = \frac{(H_{s,swell}/4)^{2}}{(\lambda)\sqrt{2\pi}} \cdot exp\left\{-\frac{\left(\omega - \omega_{p},swell\right)^{2}}{2(\lambda)^{2}}\right\} \tag{9}$$

[2] Considering an in air environment

This is in agreement with various guidelines for the marine industry (e.g. [55-56]). The directionality of the two spectra was fixed at a 180 degrees heading for wind seas and a 90 degrees heading for swell. It was assumed that wind driven and swell seas are long-crested and generate only normal and shear stresses, respectively. Additionally, it was assumed that stress spectral density functions are the same as wave spectra - meaning that unit response amplitude operators were assumed. Normally, multiplication of the wave spectra with response amplitude operators slightly shifts the spectra towards another frequency range. Therefore, it was necessary to choose the spectra parameters such that they correspond to a realistic structural response of a typical marine structure. The used spectra parameters are listed in Tab. 4 and the corresponding energy density spectra are depicted in Fig. 6.

The selected VA case is representative for a general fillet welded connection in a marine structure (see Fig. 7). It is supposed that along the weld a multiaxial stress state is generated consisting of a normal stress induced by wind seas and a shear stress induced by a simultaneous swell.

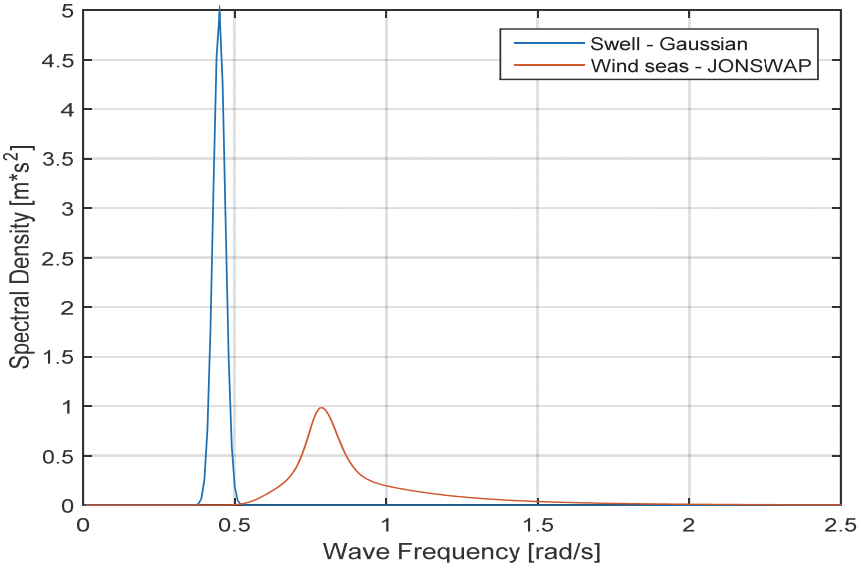

Figure 6: Energy density for wind seas and swell.

Parameter	Description	Value
$T_{p,wind}$	*Peak period of wind seas*	$8\,s$
$T_{p,\ swell}$	*Peak period of swell seas*	$14\,s$
$H_{s,wind}$	*Significant wave height of wind seas*	$2\,m$
$H_{s,swell}$	*Significant wave height of swell seas*	$2\,m$
g	*Gravitational constant*	$9.81\,m/s^2$
λ	*Gaussian spectral width*	0.02
γ	*Peakedness factor of JONSWAP spectrum*	3.3

Table 4: All parameters which have been used to describe the two spectra of swell respectively wind seas.

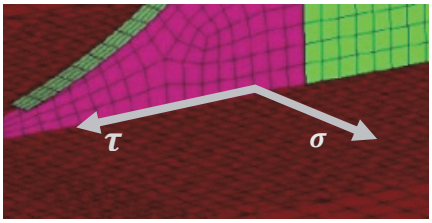

Figure 7: Illustration of the local multiaxial stress components (normal and shear) with respect to a structural detail

FATIGUE LIFETIME ESTIMATION

Multiaxial cycle counting

The intricacy in processing the generated time traces lies in the cycle counting procedure. The authors used their own multiaxial cycle counting algorithm developed based on publications of the PDMR cycle counting method [52, 57, 58]. This algorithm was used to process time traces of normal and shear nominal stress which were generated with the two considered wave spectra. The generated time traces were scaled with four different stress amplitude ratios $\left\{\frac{\tau_A}{\sigma_A}=\frac{1}{1};\frac{\tau_A}{\sigma_A}=\frac{1}{2};\frac{\tau_A}{\sigma_A}=\frac{1}{3};\frac{\tau_A}{\sigma_A}=\frac{1}{5};\right\}$ and then PDMR counted in $\sigma-\sqrt{3}\tau$ stress space.

Multiaxial damage accumulation

For quantitative comparison, the PDMR cycle counting results were converted into an accumulated damage and then normalized with respect to pure normal stress. For this purpose Miner's linear damage accumulation rule was used in combination with a reference SN-curve. This reference SN-curve had to be compatible with the PDMR based cycle counting. Therefore, the selected experimental data from [3] was used again. For the four load cases (i.e. pure bending, pure torsion, combined IP loading and combined OP loading) the corresponding effective stress range was determined using PDMR cycle counting. In this case, these effective stress ranges correspond with the half-length of the load path in $\sigma-\sqrt{3}\tau$ stress-space. Eventually, a mean SN-curve was establishing by making a linear regression as shown in Fig. 8. Tab. 5 lists the parameters of the mean SN-curve. Accumulated fatigue damage was then calculated using the mean minus two times standard deviation SN-curve.

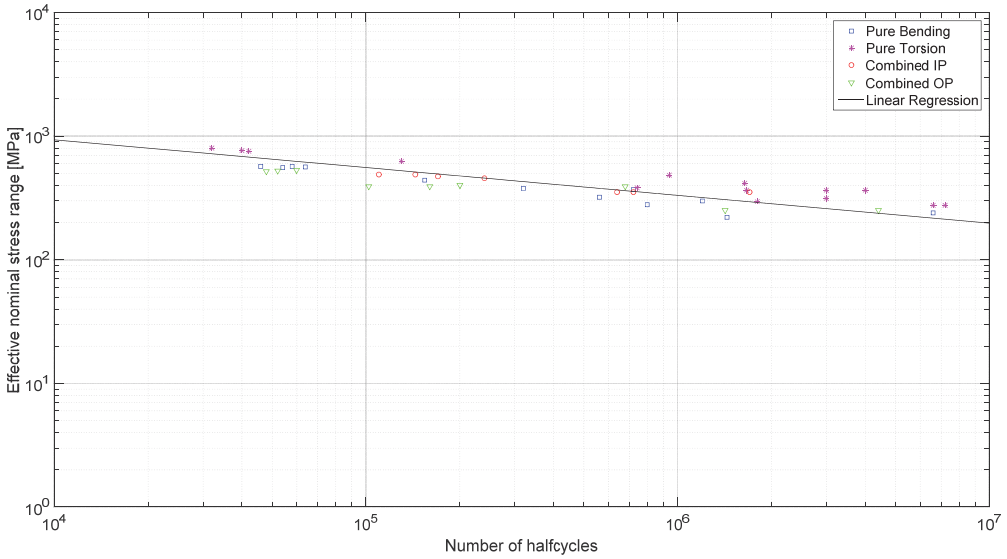

Figure 8: Mean SN-curve used to determine the accumulated fatigue data and generated using data published in [3].

Parameter	Value
$log(C)$	17.2
m	4.45
SD	0.369

Table 5: Parameters of mean SN-curve.

For comparison the CA load cases were also analysed using the PDMR based approach. The normalized results are listed in Tab. 6 and show that the virtual path length, which is identified in this counting procedure, has a large effect on the damage calculation. For the VA load cases twenty minute time traces were used of which a part of a typical realization is shown in Fig. 9. In Fig. 10 an example is given of a VA multiaxial load path considering an amplitude ratio of 1.
Fig. 11 shows the histograms that resulted from PDMR cycle counting of the load path depicted in Fig. 10 when the virtual path length is included and excluded. Again a significant impact of the virtual load path on the accumulated fatigue damage was observed. Furthermore, a peak is observed at very low stress ranges. This is caused by all the remaining small pieces of path length that result from 'cutting' the load path in the counting procedure. For twenty realizations the average fatigue damage was calculated using PDMR cycle counting including and excluding the virtual path length. The values were normalized with pure tension/bending (i.e. normal stress only) and are listed in Tab. 7a. Multiple realizations were needed because of unknown phases between the individual frequency components of the stress spectra.

					LC 5	
PDMR based method	LC 1	LC 2	LC 3	LC 4	*Including virtual path*	*Excluding virtual path*
Normalized damage	1.0	1.0	5.0	6.7	38	7.1
Normalized path length	1.0	1.0	1.4	1.5	2.7	2.2
Scaled maximum range	2.0	2.0	2.8	3.1	5.2	3.2
Number of half cycles	2	2	2	2	4	4

Table 6: Fatigue damage (info) obtained with PDMR cycle counting for CA load cases; Results normalized with pure tension/bending

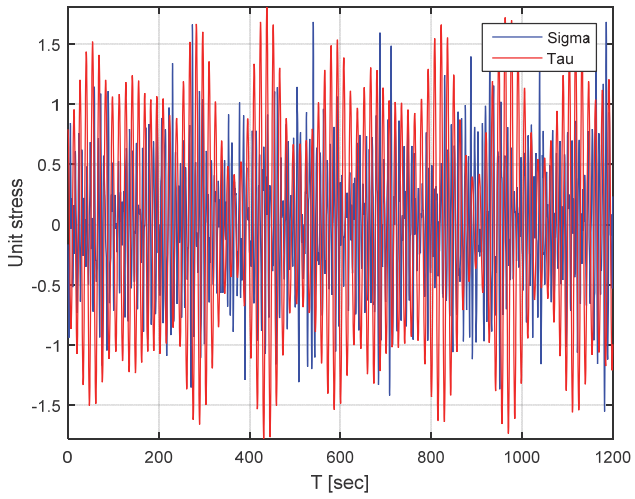

Figure 9: Example of two typical time traces for sigma and tau which have been used for PDMR based cycle counting.

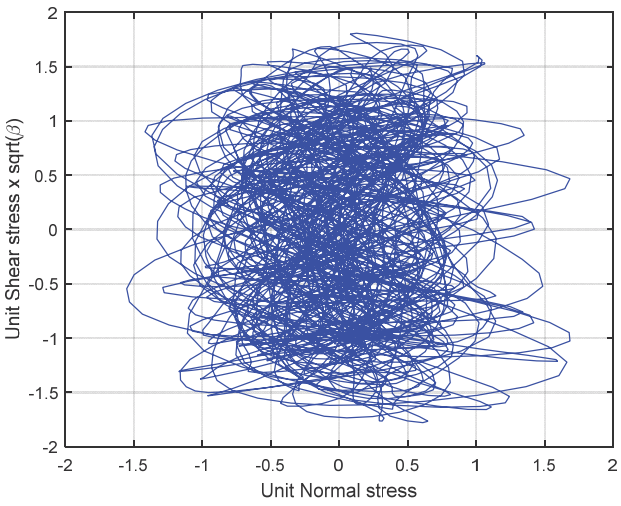

Figure 10: Multiaxial load path of a twenty minute time trace from a three hour realization depicted in the $\sigma - \sqrt{3}\tau$ stress space whilst considering a stress amplitude ratio of 1.

Stress amplitude ratio τ_A/σ_A	1:5	1:3	1:2	1:1
D_{avg} *including virtual path*	2.7	5.0	5.5	52
D_{avg} *excluding virtual path*	1.5	2.3	2.1	25

Table 7a: Average fatigue damage obtained with PDMR cycle counting for VA loading considering different stress amplitude ratios; Results normalized with pure tension/bending (i.e. normal stress only).

From the results obtained from the VA load cases an exponential trend was inferred between stress amplitude ratio and fatigue damage. Therefore, an additional damage calculation was executed with a stress ratio of 0.8. The results are listed and compared with the other stress amplitude ratio's in Tab. 7b. An exponential increase of fatigue damage is indeed clearly shown in Fig. 12. The power functions that corresponds with the two fitting curves correspond with the generic Eq. 11.

$$y = a \cdot x^b \begin{cases} a = 50, b = 3.1 \, excluding \, virtual \;\; path \\ a = 24, b = 3.1 \, including \, virtual \;\; path \end{cases} \tag{11}$$

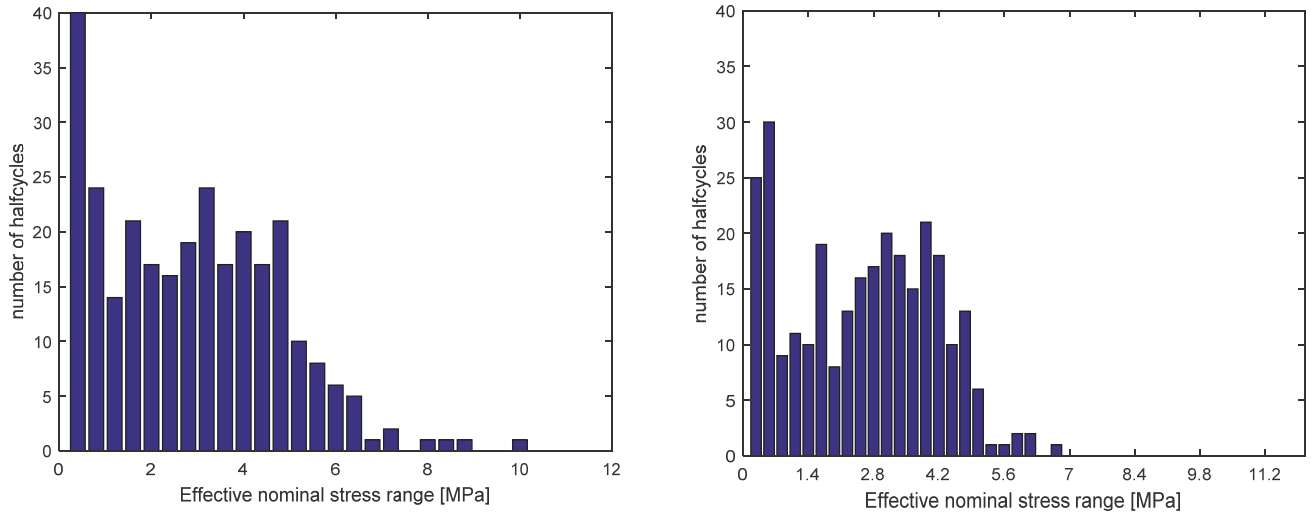

Figure 11: Histograms resulting from PDMR cycle counting of the load path depicted in Fig. 4 (right); Virtual path included (left) and excluded (right).

Stress amplitude ratio τ_A/σ_A	1:5	1:3	1:2	4:5	1:1
D_{avg} *including virtual path*	2.7	5.0	5.5	29	52
D_{avg} *excluding virtual path*	1.5	2.3	2.1	14	25

Table 7b: Average fatigue damage obtained with PDMR cycle counting for VA loading; Results normalized with pure tension/bending (i.e. normal stress only).

DISCUSSION

From the three investigated codes it is found that Eurocode 3 does not distinguish between proportional (LC3) and non-proportional (LC4) loadings while IIW does. This is resulting from the use of different critical values in their fatigue criterion. Incorporating frequency induced non-proportionality using the conservative strategy (LC5.1), results in a doubling of the normalized damage obtained under phase shift induced non-proportionality. Interestingly, using the alternative strategy (i.e. LC5.2), Eurocode results in a higher damage, while IIW results in a lower damage than LC4. This is likely caused by the different damage mechanisms which are presumed (i.e. difference in exponents). A principal stress based approach, such as suggested by DNV-GL, results in a slight reduction of fatigue damage under non-proportional loading (LC 4 and 5) in comparison to proportional loading (LC 3) due to a reduced maximum principal stress range. Furthermore, it does not distinguish between phase shift or frequency induced non-proportionality and due to the principal stress direction dependent reference SN-curve and Mode-I based slope, pure torsional loading results in a lower damage compared to Eurocode 3 or IIW. With IIW, non-proportionality has the highest impact on fatigue damage. Comparison of the codes amongst each other per individual load case results in practically the same conclusions.
Looking at the results from the selected multiaxial fatigue methods, it appears that with the MCSC, the impact of non-proportionality on fatigue lifetime is less damaging or equally damaging to the proportional load case. The comparison between MCSC and MWCM for each individual load case lead to the same findings. However, this is in contradiction with experimental results of testing welded steel joints [3]. Possibly the procedure which was selected to determine the normal and shear stress components acting on the critical plane should be changed. Remarkable about the comparison between the normalized results for MCSC and MWCM is a factor two for all multiaxial load cases (LC3, 4 and 5), which could also be a result of this selected procedure. The MWCM is hardly capable of accounting non-proportionality due to the fact that the stress amplitude ratio does not depend on the type of loading. From the three considered multiaxial fatigue methods the EESH results seem to be most affected by (non-)proportionality. However, this method becomes more complex when VA loading is under consideration.

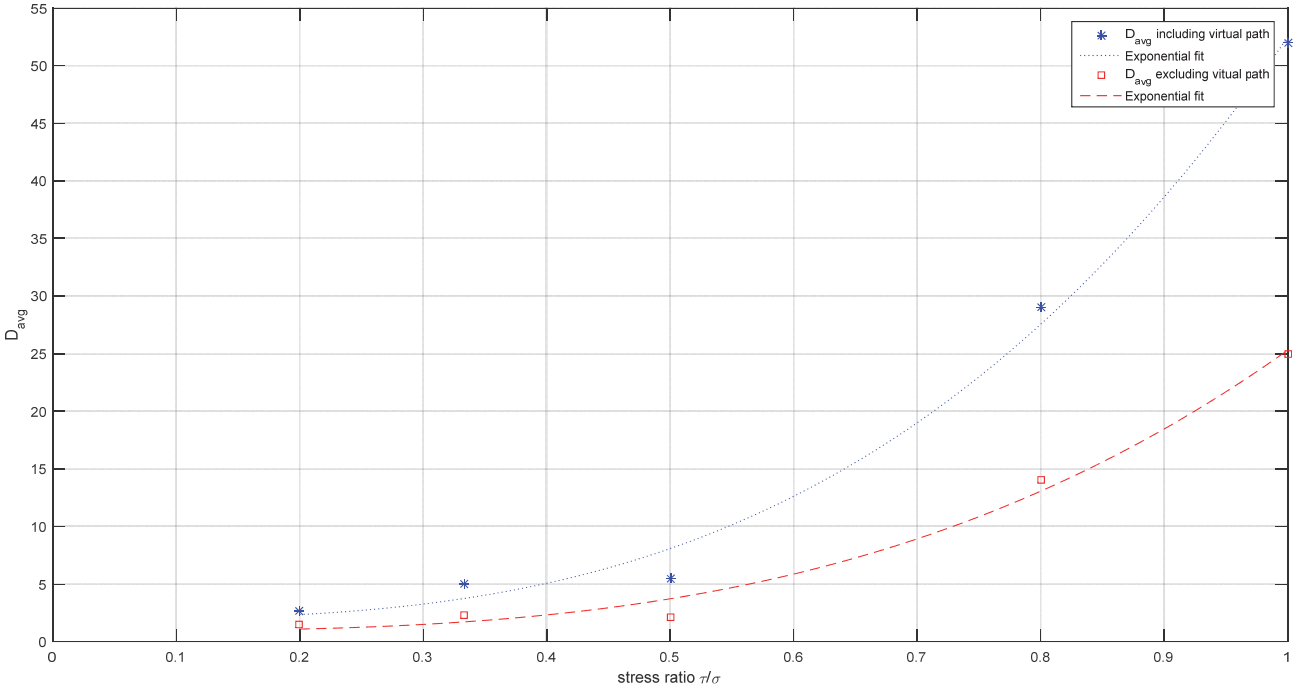

Figure 12: Graph showing the exponential increase of fatigue damage with increasing stress amplitude ratio considering PDMR based cycle counting

In the PDMR based approach the virtual load path strongly affects the damage calculations. Moreover, the averaged normalized damage sums that were obtained in this study would require more realizations to achieve full convergence for stress amplitude ratio 1:3 and 1:2. This causes the averaged damage sum at a ratio of 1:3 to be slightly higher than at a

ratio of 1:2 which seems contradictory. A non-linear relationship is observed between fatigue damage and the shear stress contribution (i.e. stress amplitude ratio) which can be described by a power function. This explains why codes and most multiaxial fatigue methods suggest a type of power function which relates fatigue damage to the two stress components: normal and shear. Analysis of the constant amplitude load cases with the PDMR based approach showed that for non-proportional load cases the increased load path in combination with the reference SN-curve results in a significant increase in the normalized fatigue damage. Interesting is that, for the VA load cases, the power coefficients of both fitting curves (Fig. 12) are smaller than the slope of the SN-curve that was used for damage calculation (Fig. 8). The PDMR model takes only the fatigue strength aspect of multiaxiallity into account. The fatigue damage mechanism parameter (slope m) is a regression based value. It represents the average effective value of the load case specific slopes of the considered experimental (fatigue resistance) data. Increasing the variety of load cases incorporated to construct the SN-curve may result into an improved average effective slope value. In this study, the SN-curve was generated with data of only 1 stress amplitude ratio. However, the calculated damage (i.e. lifetime) estimates can still be conservative or non-conservative depending on the considered load case. A complete multiaxial fatigue resistance model should take both the load case specific fatigue strength and fatigue damage mechanism into account.

CONCLUSION

In this study, a selection of codes and multiaxial fatigue methods for the marine industry were investigated considering (non-proportional) constant amplitude loading. Furthermore, a case study was developed and used to examine the relationship between variable amplitude loading and fatigue damage based on PDMR cycle counting.
From the most selected codes and multiaxial fatigue methods it appears that constant amplitude induced multiaxiallity can increase fatigue damage up to a factor of approximately four. The DNV-GL principal stress based approach seems to be on the non-conservative side while IIW could be on the conservative side. Criteria which are based on a critical plane or consider interacting material planes aim to improve fatigue lifetime estimates based on the theory of cyclic deformation in crystals.
For variable amplitude loading, a non-linear relationship (described by a power function) is observed between fatigue damage and stress amplitude ratio. Furthermore, it has been shown that virtual path lengths can strongly affect the results from PDMR based cycle counting.
It can be concluded that there are large discrepancies between the fatigue damages resulting from the application of codes, multiaxial fatigue methods and the PDMR based approach. All comparisons in this study are based on nominal stresses meaning that the use of more local stress information could improve the results. However, particularly experimental testing under (frequency induced) non-proportional multiaxial loading is expedient for validation, refinement or the development of existing and new methods. For this purpose the proposed case study provides a reasonable basis.

ACKNOWLEDGEMENTS

This work was executed as part of the 4D-Fatigue project and therefore the authors gratefully acknowledge the support from the Dutch Foundation for Technological research (STW), Industrial project participants and the Delft University of Technology.

REFERENCE

[1] Hong, J. K., Forte, T. P., Fatigue evaluation procedures for multiaxial loading in welded structures using the Battelle Structural Stress approach. In ASME 2014 33rd International Converence on Ocean, Offshore and Arctic Engineering (pp. 1–9). San Fransisco, USA, (2014).
[2] Maddox, S. J., Fatigue assessment of welds not oriented either normal or parallel to the direction of loading. Cambridge, UK, (2010).
[3] Sonsino, C. M., Kueppers, M. Multiaxial fatigue of welded joints under constant and variable amplitude loadings. Fatigue and Fracture of Engineering Materials and Structures, 24 (2001) 309–327.
[4] Anes, V., Reis, L., De Freitas, M., A new criterion for evaluating multiaxial fatigue damage under multiaxial random loading conditions. In Fatigue 2014. Melbourne, Australia: Fatigue 2014, (2014).

[5] Meggiolaro, M. A., Tupiassú, J., De Castro, P., An improved multiaxial rainflow algorithm for non-proportional stress or strain histories - Part II: The Modified Wang-Brown method. International Journal of Fatigue, (2011). http://doi.org/10.1016/j.ijfatigue.2011.10.012.
[6] Wei, Z., Dong, P., Batra, R. C., Nikbin, K., Analysis of multi-axial test data using a path-dependent effective stress/strain definition. In ASME 2013 Pressure Vessels and Piping Conference. Paris, France: PVP2013-97630, (2013).
[7] Carpinteri, A., Spagnoli, A., Vantadori, S., Multiaxial fatigue life estimation in welded joints using the critical plane approach. International Journal of Fatigue, 31 (2008) 188–196. http://doi.org/10.1016/j.ijfatigue.2008.03.024.
[8] Li, J., Zhang, Z.-P., Sun, Q., Li, C.-W., Multiaxial fatigue life prediction for various metallic materials based on the critical plane approach. International Journal of Fatigue, 33 (2011) 90–101. http://doi.org/10.1016/j.ijfatigue.2010.07.003.
[9] Susmel, L., Tovo, R., On the use of nominal stresses to predict the fatigue strength of welded joints under biaxial cyclic loading. Fatigue Fracture of Engineering Materials Structures, 27 (2004) 1005–1024. http://doi.org/10.1111/j.1460-2695.2004.00814.x.
[10] Cristofori, A., Susmel, L., Tovo, R., A stress invariant based criterion to estimate fatigue damage under multiaxial loading. International Journal of Fatigue, 30 (2007) 1646–1658. http://doi.org/10.1016/j.ijfatigue.2007.11.006.
[11] Macha, E., Sonsino, C. M., Energy criteria of multiaxial fatigue failure. Fatigue and Fracture of Engineering Materials and Structures, 22 (1999) 1053–1070.
[12] Niesłony, A., Comparison of some selected multiaxial fatigue failure criteria dedicated for spectral method. Journal of Theoretical and Applied Mechanics, 48(1) (2010) 233–254.
[13] Wang, Y.-Y., Yao, W.-X. Evaluation and comparison of several multiaxial fatigue criteria. International Journal of Fatigue, 26 (2004) 17–25. http://doi.org/10.1016/S0142-1123(03)00110-5.
[14] Besten, J. H. den. A total stress concept. Delft University of Technology, (2015).
[15] Suresh, S., Fatigue of materials (Second edi). Cambridge, UK: Cambridge University Press, (1998).
[16] Callens, A., Bignonnet, Fatigue design of welded bicycle frames using a multiaxial criterion. Procedia Engineering, 34 (2012) 640–645. http://doi.org/10.1016/j.proeng.2012.04.109.
[17] Dang Van, K., On a unified fatigue modelling for structural analysis based on the shakedown concept. Mecamix, X-Tech. Paris, France, (2014).
[18] Lieshout, P. S. van, Besten, J. H. den, Kaminski, M. L., Validation of the corrected Dang Van multiaxial fatigue criterion applied to turret bearings of FPSO offloading buoys. Ships and Offshore Structures, to be publ., (2016).
[19] Radaj, D., Sonsino, C. M., Fricke, W., Fatigue assessment of welded joints by local approaches. Woodhead Publishing Limited, 53 (2006). http://doi.org/10.1017/CBO9781107415324.004.
[20] Susmel, L., Lazzarin, P. A bi-parametric Wöhler curve for high cycle multiaxial fatigue assessment. Fatigue and Fracture of Engineering Materials and Structures, 25(1) (2002) 63–78. http://doi.org/10.1046/j.1460-2695.2002.00462.x
[21] DNV-GL.,Fatigue design of offshore steel structures. Recommended Practice DNVGL-RP-0005:2014-06, 1–126. (2005). Retrieved from ftp://128.84.241.91/tmp/MSE-4020/Fatigue-Design-Offshore.pdf
[22] Eurocode 3. Design of steel structures - Part 1-9: Fatigue. (2005).
[23] Hobbacher, A., Recomendations for Fatigue Design of Welded Joints and Components. IIW document IIW-1823-07 ex XIII-2151r4-07/XV-1254r4-07. Paris, France, (2008).
[24] Farajian, M., Nitschke-Pagel, T., Boin, M., Wimpory, R. C., Relaxation of welding residual stresses in tubular joints under multiaxial loading. The Tenth International Conference on Multiaxial Fatigue Fracture (ICMFF10), (2013).
[25] Backstrom, M., Marquis, G., Interaction equations for multiaxial fatigue assessment of welded structures. Fatigue and Fracture of Engineering Materials and Structures, 27 (2004) 991–1003. http://doi.org/10.1111/j.1460-2695.2004.00811.x.
[26] Gaier, C., Dannbauer, H., An Efficient Critical Plane Method for Ductile , Semi- Ductile and Brittle Materials. In Oral reference: FT436. Elsevier Ltd. (2006).
[27] Papadopoulos, I. V., Panoskaltsis, V. P., Gradient-Dependent Multiaxial High-Cycle Fatigue Criterion. Multiaxial Fatigue and Design, ESIS 21, Edited by A. Pineau, G. Caileetaud, and T. C. Lindley, (1996).
[28] Gustafsson, J., Multi-axial fatigue in welded details-An investigation of existing design approaches. Chalmers University of Technology, (2007).
[29] Wang, Y., Susmel, L., The Modified Manson–Coffin Curve Method to estimate fatigue lifetime under complex constant and variable amplitude multiaxial fatigue loading. International Journal of Fatigue, 83 (2016) 135–149. http://doi.org/10.1016/j.ijfatigue.2015.10.005.

[30] Carpinteri, A., Brighenti, R., Macha, E., Spagnoli, A., Expected principal stress directions under multiaxial random loading. Part II: numerical simulation and experimental assessment through the weight function method. International Journal of Fatigue, 21 (1999) 89–96.
[31] Carpinteri, A., Spagnoli, A., Multiaxial high-cycle fatigue criterion for hard metals. International Journal of Fatigue, 23 (2001) 135–145. Retrieved from www.elsevier.com/locate/ijfatigue.
[32] Ronchei, C., Carpinteri, A., Fortese, G., Spagnoli, A., Vantadori, S., Kurek, M., Lagoda, T., Life estimation by varying the critical plane orientation in the modified Carpinteri-Spagnoli criterion. Frattura Ed Integrita Strutturale, 9(34) (2015) 74–79. http://doi.org/10.3221/IGF-ESIS.34.07.
[33] Papadopoulos, I., Critical Plane Approaches in High-Cycle Fatigue: on the Definition of the Amplitude and Mean Value of the Shear Stress Acting on the Critical Plane. Fatigue Fracture of Engineering Materials Structures, 21(3) (1998) 269–285. http://doi.org/doi:10.1046/j.1460-2695.1998.00459.x.
[34] Susmel, L., Tovo, R., Benasciutti, D., A novel engineering method based on the critical plane concept to estimate the lifetime of weldments subjected to variable amplitude multiaxial fatigue loading. Fatigue and Fracture of Engineering Materials and Structures, 32 (2009) 441–459. http://doi.org/10.1111/j.1460-2695.2009.01349.x.
[35] Susmel, L., A simple and efficient numerical algorithm to determine the orientation of the critical plane in multiaxial fatigue problems. International Journal of Fatigue, 32 (2010) 1875–1883. http://doi.org/10.1016/j.ijfatigue.2010.05.004.
[36] Sonsino, C. M., Multiaxial fatigue of welded joints under in-phase and out-of-phase local strains and stresses. International Journal of Fatigue, 17 (1995) 55–70.
[37] Sonsino, C. M., Wiebesiek, J., Assessment of multiaxial spectrum loading of welded streel and aluminium joints by modified equivalent stress and gough-pollard algorithms. Darmstadt, Germany, (2007).
[38] Backstrom, M., Multiaxial fatigue life assessment of welds based on nominal and hot spot stresses. Lappeenranta University of Technology, Lappeenranta, Finland, (2003).
[39] Fricke, W., Recommended Hot Spot Analysis Procedure for Structural Details of FPSOs and Ships Based on Round-Robin FE Analyses. In 11th Internation Offshore and Polar Engineering Conference. Stavanger, Norway, (2001).
[40] Maddox, S. J., Recommended Hot-Spot Stress Design S-N Curves for Fatigue Assessment of FPSOs. In 11th International Offshore and Polar Engineering Conference. Stavanger, Norway, (2001).
[41] Maddox, S. J., Hot-Spot Stress Design Curves for Fatigue Assessment of Welded Structures. International Journal of Offshore and Polar Engineering, 12(2) (2002) 1053–5381.
[42] Kyuba, H., Dong, P. Equilibrium-equivalent structural stress approach to fatigue analysis of a rectangular hollow section joint. International Journal of Fatigue, 27 (2005) 85–94. http://doi.org/10.1016/j.ijfatigue.2004.05.008.
[43] Selvakumar, P., Hong, J. K., Robust Mesh Insensitive Structural Stress Method for Fatigue Analysis of Welded Structures. Procedia Engineering, 55 (2013) 374–379. http://doi.org/10.1016/j.proeng.2013.03.268.
[44] Tveiten, B. W., Moan, T., Determination of structural stress for fatigue assessment of welded aluminum ship details. Marine Structures, 13 (2000) 189–212. http://doi.org/10.1016/S0951-8339(00)00022-8.
[45] Pedersen, M. M., Multiaxial fatigue assessment of welded joints using the notch stress approach. International Journal of Fatigue, 83 (2016) 269–279. http://doi.org/10.1016/j.ijfatigue.2015.10.021.
[46] Radaj, D., Sonsino, C. M., Fricke, W., Recent developments in local concepts of fatigue assessment of welded joints. International Journal of Fatigue, 31 (2008) 2–11. http://doi.org/10.1016/j.ijfatigue.2008.05.019.
[47] Sonsino, C. M., Fricke, W., De Bruyne, F., Hoppe, A., Ahmadi, A., Zhang, G., Notch stress concepts for the fatigue assessment of welded joints - Background and applications. International Journal of Fatigue, 34 (2012) 2–16. http://doi.org/10.1016/j.ijfatigue.2010.04.011.
[48] Exel, N., Sonsino, C. M., Multiaxial fatigue evaluation of laserbeam-welded magnesium joints according to IIW-fatigue design recommendations. Welding in the World, 58(4) (2014) 539–545. http://doi.org/10.1007/s40194-014-0139-6.
[49] Anes, V., Reis, L., Li, B., De Freitas, M., New cycle counting method for multiaxial fatigue. International Journal of Fatigue, (2014). http://doi.org/10.1016/j.ijfatigue.2014.02.010.
[50] Anes, V., Reis, L., Li, B., Fonte, M., De Freitas, M., New approach for analysis of complex multiaxial loading paths. International Journal of Fatigue, 62 (2014) 21–33. http://doi.org/10.1016/j.ijfatigue.2013.05.004
[51] Mamiya, E. N., Castro, F. C., Malcher, L., Araújo, J. A., Multiaxial fatigue life estimation based on combined deviatoric strain amplitudes. International Journal of Fatigue, 67 (2014) 117–122. http://doi.org/10.1016/j.ijfatigue.2013.11.002.
[52] Dong, P., Wei, Z., Hong, J. K., A path-dependent cycle counting method for variable-amplitude multi-axial loading. International Journal of Fatigue, 32 (2009) 720–734. http://doi.org/10.1016/j.ijfatigue.2009.10.010.

[53] Zou, T., Kaminski, M. L., Validation of WaveWatch-III wave model for investigation of climate change effects on fatigue lifetime of offshore floating structures 2 Wave data formats. To Be Published. (2016).
[54] Journée, J. M. J., Pinkster, J., Introduction in Ship Hydromechanics. TU Delft, 1 (2002). http://doi.org/10.1111/ejh.12375.
[55] DNV. Environmental Conditions and Environmental Loads, (2010).
[56] Kim, B., Wang, X., Shin, Y.-S., Extreme load and fatigue damage on FPSO in combined waves and swells. ABS Technical papers. Houston, Texas, (2007).
[57] Wei, Z., Dong, P., A rapid path-length searching procedure for multi-axial fatigue cycle counting. Fatigue and Fracture of Engineering Materials and Structures, 35 (2011) 556–571. http://doi.org/10.1111/j.1460-2695.2012.01649.x.
[58] Wei, Z., Dong, P., A generalized cycle counting criterion for arbitrary multi-axial fatigue loading conditions, Journal of Strain Analysis for Engineering Design, 49 (2014) 325–341.